On the forced flow around a rigid flapping foil

F. Mandujano, and C. Málaga

Citation: Physics of Fluids **30**, 061901 (2018); doi: 10.1063/1.5026102
View online: https://doi.org/10.1063/1.5026102
View Table of Contents: http://aip.scitation.org/toc/phf/30/6
Published by the American Institute of Physics

On the forced flow around a rigid flapping foil

F. Mandujano and C. Málaga[a)]
Physics Department, National Autonomous University of Mexico, Mexico City, Mexico

(Received 15 February 2018; accepted 8 June 2018; published online 26 June 2018)

The two dimensional incompressible viscous flow past a flapping rigid foil immersed in a uniform stream is studied using a lattice-Boltzmann model. When the foil's center of mass is fixed in space, numerical results reproduce the transition from the von Kármán (vKm) to the inverted von Kármán wake [T. Schnipper, A. Andersen, and T. Bohr, "Vortex wakes of a flapping foil," J. Fluid Mech. **633**, 411 (2009) and A. Das, R. K. Shukla, and R. N. Govardhan, "Existence of a sharp transition in the peak propulsive efficiency of a low pitching foil," J. Fluid Mech. **800**, 307 (2016)]. Beyond the inverted vKm transition, the foil was released. The numerical results show that the hydrodynamic forces on the flapper are oscillatory functions of time with amplitudes and mean values that scale with the square of the Strouhal number, defined with either the flapping amplitude or the flapper length that decays an order of magnitude when the foil is freed to swim. Upstream swimming consisted of a uniform horizontal motion and a vertical heaving. The swimming speed showed a linear dependence on the Strouhal number, defined with the amplitude of oscillation of the foil tip. As a consequence, thrust generated by the free flapper is related to the square of the swimming speed for moderate Reynolds numbers. *Published by AIP Publishing.* https://doi.org/10.1063/1.5026102

I. INTRODUCTION

The flow around a flapping foil has been studied under a variety of conditions. Foils on a stream, flapping as a result of the hydrodynamic forces acting on them, have been studied in connection to energy extraction processes.[3,4] The wake behind foils with an imposed flapping and translational motion, and its relation with the reacting forces on them has deserved attention due to its relation to flying and swimming.[5–8] Little has been done in the case of an imposed flapping on a foil free to swim in a quiescent fluid[9–11] and against a stream in a uniform flow although work can be found related to other types of swimmers at moderate Reynolds numbers.[12–14]

Here we numerically study a two-dimensional rigid foil[1,2,15] with an imposed flapping motion, immersed in a stream, that can be released and become free of translational motion. Both phenomena were studied and compared for moderate Reynolds numbers, where inertia and viscous forces are important. In contrast to the work of Vanderberghe *et al.*[9] and Alben and Shelley,[10] in which the foil and the imposed flapping motion have fore and aft symmetry and swimming motion results from a symmetry breaking of the flow generated, our foil and flapping do not have such a symmetry and swimming motion occurs always against the imposed uniform stream.

We used a lattice Boltzmann model (LBM),[16] with a procedure to include the immersed moving boundaries of arbitrary shape subject to hydrodynamic forces.[17] The LBM is an efficient algorithm to approximate solutions to the Navier-Stokes equations when implemented on massively parallel architectures, where it can handle the simulations of high resolution and large computational domains.[18] For the problem in hand, the LBM seemed a good option since wakes behind objects may show interesting behavior far away behind the object,[19] and so a large domain relative to the size of the foil was desirable, along with enough resolution to observe vortex formation and evolution.

This article is divided as follows: in Sec. II, the general problem is presented, and the numerical method used is described briefly in Sec. III. In Sec. IV, the results are presented and discussed. Conclusions are summarized in Sec. VI.

II. STATEMENT OF THE PROBLEM

Consider an unbounded two dimensional and incompressible flow of a viscous fluid around a rigid flapping foil in the form of a semicircle, with diameter D, intersected with an isosceles triangle of height h, as shown in Fig. 1. This simplified profile was used in Refs. 1, 15, and 20 and was chosen to validate our numerical results. Two cases are considered, a foil with a point fixed in space and a foil free to move. In both cases, the flapping motion consists of an oscillation with respect to the center of the semicircle, which is fixed in space in one case and free in the other. To simplify the calculations, it is assumed that the foil mass density distribution, ρ_s, is such that its center of mass is at the center of the semicircle. In this way, the translational motion is decoupled from the imposed pitching, and motions such as heaving are the result of hydrodynamic interactions only. A study of the effects due to the position of the pivot relative to the center of mass can be found in Ref. 21.

The governing equations for the fluid, with mass density ρ_f and kinematic viscosity ν, are the Navies-Stokes equations which are given by

$$\nabla \cdot \boldsymbol{u} = 0, \tag{1}$$

$$\frac{\partial \boldsymbol{u}}{\partial t} + \boldsymbol{u} \cdot \nabla \boldsymbol{u} = -\frac{1}{\rho_f} \nabla P + \nu \nabla^2 \boldsymbol{u}, \tag{2}$$

a)cmi.ciencias@ciencias.unam.mx.

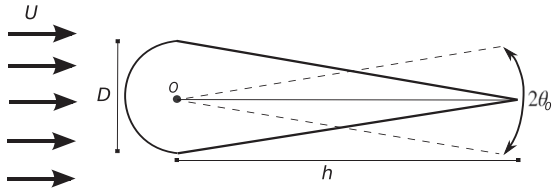

FIG. 1. Schematic illustration of the flow around a rigid flapping foil. The axle of rotation is indicated by O, and $2\theta_0$ is the maximum angle of rotation with respect to O.

where $\boldsymbol{u}(\boldsymbol{r}, t)$ and $P(\boldsymbol{r}, t)$ are the velocity and pressure fields, respectively. Consider the no-slip condition at the foil's surface. Constant pressure and a uniform and horizontal velocity field $\boldsymbol{U}$ are imposed far from the foil (see Fig. 1).

The rigid foil is forced to rotate around the center of the semicircle (also its center of mass) so that the angle of its axis of symmetry with respect to the horizontal coordinate evolves with $\theta(t) = \theta_0 \sin \omega t$ (see Fig. 1). The velocity of a point at the foil's surface is $\boldsymbol{v}_s(\mathbf{r}_s, t) = \boldsymbol{V}(t) + \dot{\theta}(t)(\boldsymbol{r}_s - \boldsymbol{R})$, where $\boldsymbol{R}$ is the position of the center of mass, $\boldsymbol{V}$ is its velocity, and $\boldsymbol{r}_s$ is the position of a point at the foil's surface. Therefore, the no-slip boundary condition takes the form $\boldsymbol{u}(\boldsymbol{r}_s, t) = \boldsymbol{v}_s(\boldsymbol{r}_s, t)$. In the case of the free flapping foil, the motion of its center of mass is obtained by solving $m d\boldsymbol{V}/dt = \boldsymbol{F}$, where m is the mass of the foil. The hydrodynamical force $\boldsymbol{F}$ acting on the foil is obtained directly from the computed flow fields.

To work with non-dimensional variables, we choose D as the characteristic length, U as the characteristic velocity, and ρ_f as the fluid density. With this choice of scaling, the flow regime is determined by using five dimensionless parameters: the Reynolds number $Re = UD/\nu$, the Strouhal number $St = \omega D/2\pi U$, the dimensionless amplitude $A = 2\theta_0 h/D$, the ratio between the chord of the foil and the circle's diameter $C = 1/2 + h/D$, and the fluid-foil's mass density ratio $\mu = \rho_f/\rho_s$ which is set to unity, to reduce the number of parameters to explore. The hydrodynamic force is scaled with $\rho_f U^2 D/2$. We define the drag C_D and lift C_L coefficients as the horizontal and vertical components of $2\boldsymbol{F}/\rho_f U^2 D$, respectively. We also define the torque coefficient C_T as the hydrodynamic torque scaled with $\rho_f U^2 D^2/2$.

Solutions to Eqs. (1) and (2) for the pressure and velocity fields are approximated using a lattice-Boltzmann model. The numerical procedures are described in Sec. III.

III. THE NUMERICAL SCHEME

To compute the flow around the flapping foil, a two dimensional, nine neighbor (D2Q9) lattice-Boltzmann model was used.[16] The proposed algorithm, which includes moving immersed boundaries, was validated in a previous study concerning a problem of a moving cylinder in a convective flow.[17]

In this method, space is discretized using a square lattice. Lattice spacing as well as time steps can be conveniently set to unity. The state of the fluid at the node with vector position $\boldsymbol{r}$ at time t is described by the particle distribution function $f_k(\boldsymbol{r}, t)$ that evolves in time and space according to

$$f_k(\boldsymbol{r} + \boldsymbol{e}_k, t + 1) = f_k(\boldsymbol{r}, t) - \frac{1}{\tau}\left[f_k(\boldsymbol{r}, t) - f_k^{(eq)}(\boldsymbol{r}, t)\right], \quad (3)$$

where τ is the relaxation time related to the fluid kinematic viscosity $\nu = (\tau - 1/2)/3$. The distribution function $f_k^{(eq)}$ is given by

$$f_k^{(eq)}(\boldsymbol{r}, t) = w_k \rho\left(1 + 3\boldsymbol{e}_k \cdot \boldsymbol{u} + \frac{9}{2}(\boldsymbol{e}_k \cdot \boldsymbol{u})^2 - \frac{3}{2}\boldsymbol{u}^2\right), \quad (4)$$

which corresponds to a discrete Maxwell distribution function for thermal equilibrium. In the above expressions, the macroscopic density and velocity fields are computed using

$$\rho(\boldsymbol{r}, t) = \sum_k f_k(\boldsymbol{r}, t) \quad \text{and} \quad \rho\boldsymbol{u}(\boldsymbol{r}, t) = \sum_k \boldsymbol{e}_k f_k(\boldsymbol{r}, t).$$

The microscopic set of velocities $\boldsymbol{e}_k$ is given by

$$\begin{aligned}
\boldsymbol{e}_0 &= (0, 0),\\
\boldsymbol{e}_k &= (\cos(\pi(k-1)/2), \sin(\pi(k-1)/2)),\\
&\quad \text{for } k = 1, \ldots, 4,\\
\boldsymbol{e}_k &= \sqrt{2}(\cos(\pi(k-9/2)/2), \sin(\pi(k-9/2)/2)),\\
&\quad \text{for } k = 5, \ldots, 8,
\end{aligned}$$

where $w_0 = 4/9$ and $w_k = 1/9$ for $k = 1, \ldots, 4$ and $w_k = 1/36$ for $k = 5, \ldots, 8$. Notice that, with the choice of microscopic velocities $\boldsymbol{e}_k$, expression (3) is always evaluated at lattice points. It is well known that the above procedure approximates solutions to the Navier-Stokes equations in the limit of small Mach numbers.[16]

Equation (3) provides an explicit algorithm for updating all the distribution functions f_k at a given node in the lattice as long as its 8 nearest neighboring nodes are inside the fluid domain. For nodes adjacent to a solid wall, the distribution functions coming from the neighboring nodes outside the fluid domain must be provided as a boundary condition for the method. We choose to adopt the set of boundary conditions proposed by Guo and Zheng in Ref. 22 for curved rigid walls. In this case, the unknown distribution functions at a solid node are separated into equilibrium and non-equilibrium parts. The first is computed using a fictitious equilibrium function that enforces the boundary condition. The non-equilibrium part is approximated by that of the neighboring fluid along the link, using an interpolation scheme.

The force and torque acting on the body are computed using the momentum-exchange method of Mei *et al.* in Ref. 23. This procedure is based on the computation of the momentum exchange at the nodes adjacent to the solid boundary. The set of f_k distributions computed at these nodes using Eq. (3) and the boundary conditions is used to evaluate a change in momentum at the boundary. As f_k represents a momentum density distribution that evolves through the discretized Lagrangian time derivative expressed by Eq. (3), it can be used to approximate forces.

For the free flapper, as the rotational motion is imposed, only the force is used to compute the foil's translational motion using a forward Euler integration in time at each time step. This is a particular case of the scheme described in Ref. 17 for the motion of a free particle in a convective flow using the lattice-Boltzmann model. We must stress that the free flapper is free only of translational motion and not of rotational motion; the pitching is active, while the heaving is passive.

The computational domain was a rectangular lattice of 12 000 × 5000 nodes. The foil with a length h of 280–600 nodes and a width D of 80 nodes (about 1/30 of the width and length of the domain) was placed at 3000 nodes from the left boundary of the domain (5 foil lengths). To simulate conditions far from the foil, the velocity was set to $\boldsymbol{U}$ at the left boundary following the procedure of Ref. 22. On the rest of the boundaries, the normal components of the velocity gradients were set to zero, setting the unknown velocity at the boundary equal to that of the adjacent node normal to the wall.

The size of the domain was chosen to be big enough to ensure that the effects due to lateral walls are minimized and the internal boundary has enough number of points. For smaller domains, we found that there are important contributions to the hydrodynamic forces due to the lateral walls and the numerical errors are bigger in the neighborhood of the foil surface, which result in a fluctuating signal of the hydrodynamic force and vorticity. We found that in a domain of width bigger than six times the foil's chord h, the domain boundary effects on the forces were negligible in most of the cases. When the wake became unstable, the domain width had to be big enough to avoid the wake touching the lateral boundaries. In our experiments, a width of eight times h was enough to avoid unstable wakes to leave the domain through the horizontal boundaries.

The numerical scheme was implemented to run in parallel in GPUs due to the large number of nodes involved in the simulations. Typically, two days are needed to obtain a periodic flow (3×10^5 time steps approximately 6 flapping periods) of a free foil swimming upstream ($V_x < 0$) running on an Nvidia®Tesla K40 processor.

To test for numerical convergence, we chose a simulation of the free flapper that sheds vortices [see the inset of Fig. 2(a)]. We compared the velocity field computed for different spatial resolutions with that obtained in a fine grid. We measure the resolution with the number N of nodes that fit in the diameter D, so the reference fine grid corresponds to $N = 140$ nodes on a unit length D. To compute this difference, we used an L_2 norm of the velocity magnitude which is defined as

$$L_2 = \sqrt{\frac{1}{A}\int_\Omega |v^* - v_N|^2 ds}, \tag{5}$$

where Ω is the flow domain shown in the inset of Fig. 2(a) and A its area. The velocity magnitude v^* corresponds to the computation on a fine grid ($N = 140$), and v_N corresponds to that on a grid with N nodes per unit length D. Figure 2(a) shows L_2 for different values of $1/N$ computed at a time corresponding to the vorticity distribution shown in the inset. As N increases, the computed velocity magnitudes converge to those on the fine grid. The convergence is approximately of the second order. Figures 2(b) and 2(c) show the time evolution of the horizontal and vertical positions of the center of mass of the same free flapper computed with different values of N. Again, the solutions show convergence as the resolution increases.

IV. RESULTS

The foil profile geometry was chosen to compare with experiments performed by Ref. 1 in a soap film and by Ref. 15 in a hydrodynamic tunnel and with the numerical results in Ref. 20. The numerical results confirm the relation between the drag-trust transition and the behavior of the von Kármán (vKm) vortex street. Once the numerical scheme was validated, numerical experiments were performed for a variety of parameter values. The results of the flow around the fixed and the free foil are compared in a regime where the free foil is able to swim.

A. A fixed flapping foil

Simulations start with the foil at rest facing a uniform flow at the left boundary to allow for a wake to form before flapping. After 5×10^4 time steps (approximately one flapping period),

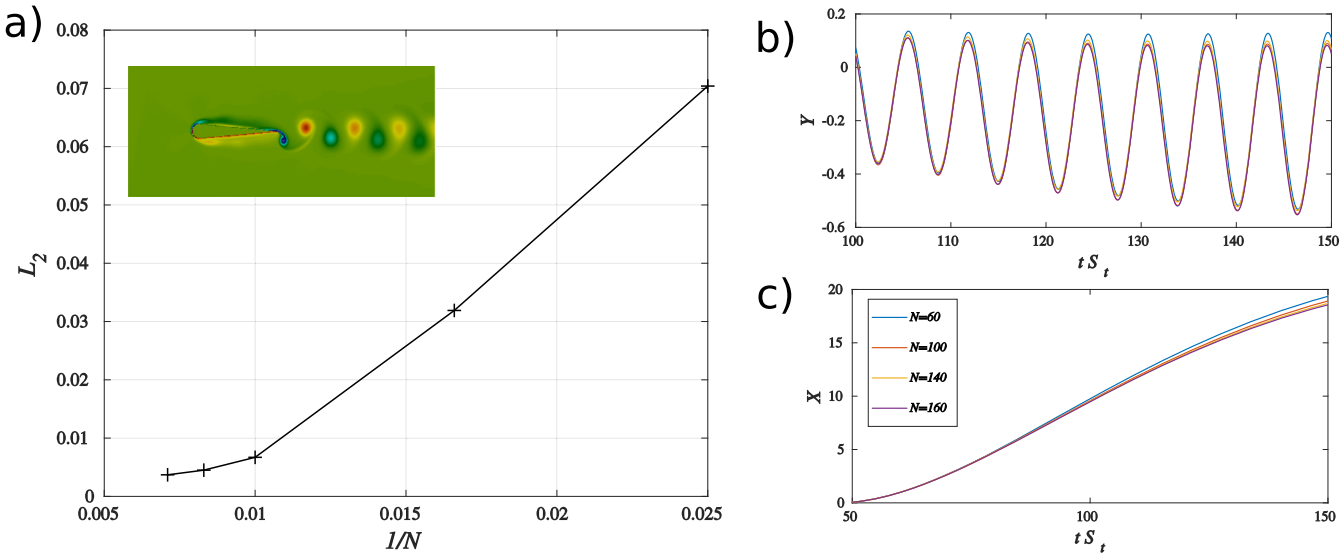

FIG. 2. (a) L_2 norm of the velocity magnitude as a function of the resolution. (b) The vertical position of the center of mass of the free flapper used in (a) vs time. (c) The horizontal position of the center of mass vs time.

the foil starts to flap increasing its amplitude exponentially in time until it reaches A, while St is kept constant at a given value. The starting protocol takes around fifty flapping periods for the exponential growth to reach the prescribed maximum or saturation value A. Following this protocol, we obtain the flow at the given values of St and A of the simulation in a non-impulsive way. The simulations were performed for a series of values of $St \in [0.1, 0.6]$, $A \in [0.5, 3]$, and $Re \in [50, 255]$, and C took values 4 and 6.

Following Ref. 1, in the first set of simulations, $Re = 220$ and $C = 6$. The simulations performed show the formation of patterns in approximately the same parameter region, as reported there (see Fig. 3). We found the same transitions between vKm and inverted vKm wake, formation of 2P, 4P, 2P + 2S, 4P + 2S wakes and the transitions between them. Following the nomenclature given in Ref. 24 where "S" represents a vortex single and "P" a vortex pair, a wake 2S + 2P means two singles and two pairs shed per cycle. The parameter values where transitions are observed in our numerical experiments differ slightly with those in Ref. 1, probably because we are simulating an infinite domain and their experiments were performed using a soap film where the flow structure is observed through the deformation of the film.

The computed hydrodynamical force on the foil showed a periodic dependence on time. When the flow has 2S or 2P wakes [Figs. 3(a)–3(c)], the lift coefficient C_L oscillates with the flapping frequency, corresponding to a Fourier mode $n = 1$. The drag coefficient C_D oscillates with twice the flapping frequency and has modes $n = 0$ and $n = 2$. When 2P, 4P, and 2S patterns appear, Fourier coefficients corresponding to higher harmonics become important. In Figs. 3(d)–3(f), the lift and torque coefficients are composed by the first few odd modes, while C_D modes are even. In the combination 2P + 2S, C_D has $n = 2$ and 4 while C_L is composed of $n = 1$ and 3 modes. The 4P wake includes modes $n = 6$ and $n = 7$, and the 4P + 2S wake has $n = 8$ and $n = 9$ modes.

For $Re \in [50, 200]$ and in the neighborhood of the transition to the inverted von Kármán wake, where thrust is expected, the computed hydrodynamic force $\mathbf{F}$ showed a sinusoidal oscillation with time. The inverted vKm transition, known to be related to the drag-thrust transition,[25] is found when the value of the product StA is between 0.15 and 0.2 for all values of Re explored, which is in good agreement with Refs. 1 and 15; StA represents the Strouhal number defined with the flapping amplitude $2h\theta_0$. In its oscillation, the minimum of the horizontal component of $\mathbf{F}$, represented by $\langle C_D \rangle - C_{DA}$, crossed zero in the interval $StA \in [0.15, 0.2]$ [see Fig. 4(a)], and this change of sign suggests that it could swim if freed. This is in contrast to earlier results, as in Ref. 20, that identify the transition when the mean drag becomes negative.

As can be seen in Fig. 4(b), the amplitude of oscillation of the drag coefficient, C_{DA}, scales roughly with the square of StA, and so the amplitude of oscillation of the horizontal component of the hydrodynamic force is proportional to the square of the characteristic tangential speed of the tip of the tail, given by $\theta_0 h\omega$. On the other hand, the average $\langle C_D \rangle$ decreases with, roughly, the square of StA. Therefore, the results suggest an estimate relation for the non-dimensional horizontal hydrodynamic force of the form

$$C_D = C_0 - \alpha(StA)^2 + \beta(StA)^2 \sin(t2St), \tag{6}$$

where α and β are dimensionless and positive factors that depend on C and Re and take the values around 2 and 3, respectively, within 25% for $C = 6$ and the values of Re explored. C_0 corresponds to the drag without flapping and varies around 0.1 within 10% for $C = 6$ and the values of Re explored.

Figure 5 shows that the amplitude of oscillation of the dimensionless lift and torque, represented by C_{LA} and C_{TA}, respectively, depends on ASt^2. Therefore, the amplitude of oscillation of the lift force F_y is proportional to $\theta_0 h(D\omega)^2$, where the length is the amplitude of flapping and $D\omega$ is the characteristic velocity of the oscillatory vertical motion of the

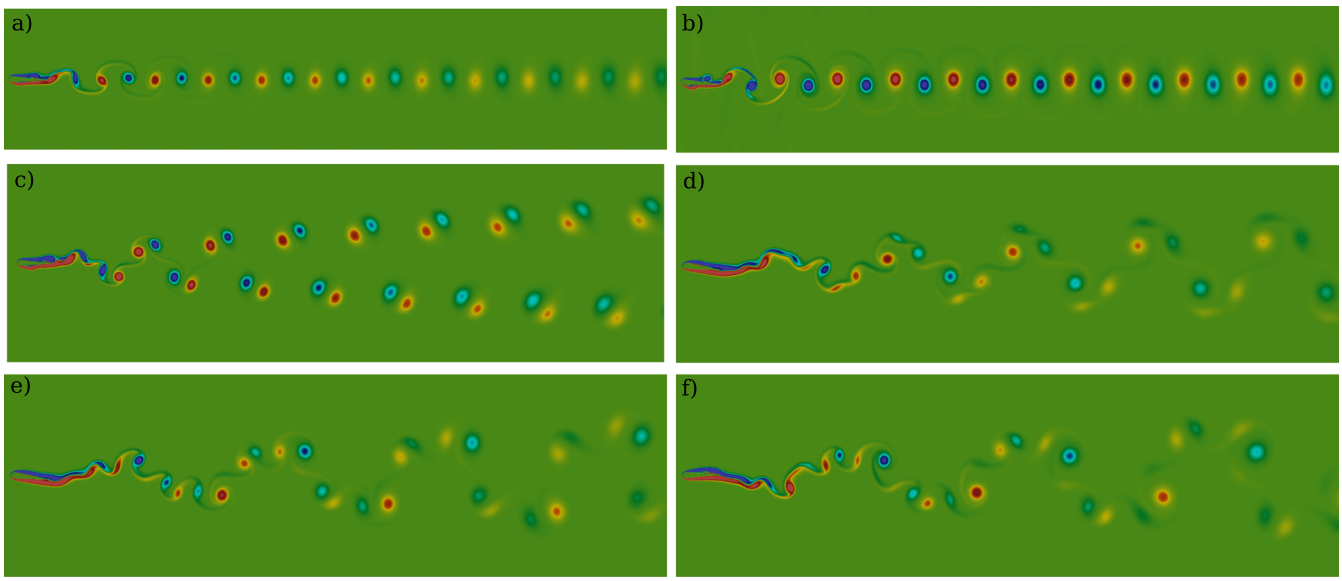

FIG. 3. Vorticity distribution for a fixed flapping foil for $Re = 220$. Colors represent positive (red) and negative (blue) vorticity. (a) vKm wake for $St = 0.12$ and $A = 0.98$. (b) Inverted vKm wake for $St = 0.12$ and $A = 2$. (c) 2P wake for $St = 0.085$ and $A = 1.4$. (d) 2P + 2S wake for $St = 0.05$ and $A = 1.4$. (e) 4P wake for $St = 0.035$ and $A = 1.34$. (f) 4P + 2S wake for $St = 0.025$ and $A = 1.2$. Only the region of interest within the computational domain is shown.

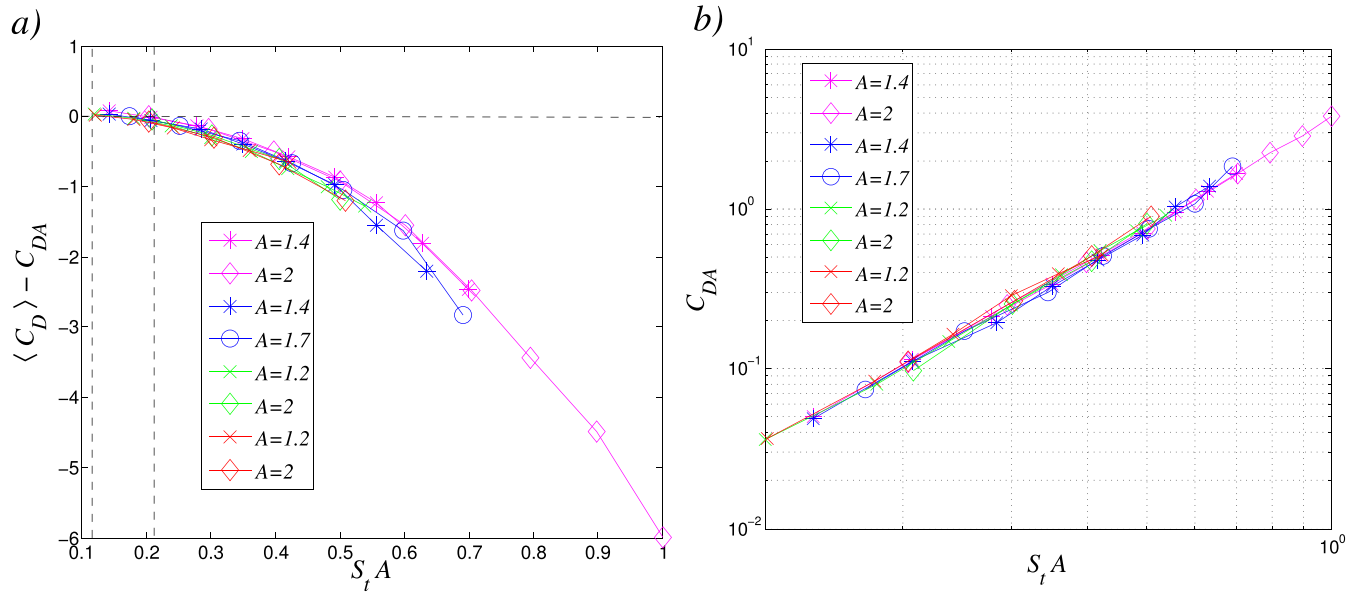

FIG. 4. Plots of the minimum drag, $\langle C_D \rangle - C_{DA}$, in (a) and of the amplitude, C_{DA}, in (b) as a function of StA. The lines connecting points mean that A was kept constant as marked. The foil's aspect ratio is $C = 6$, and the colors represent different Reynolds numbers: magenta $Re = 50$, blue $Re = 100$, green $Re = 150$, and red $Re = 200$.

foil once released (see Sec. IV B). Hence, the observations suggest the following behavior of the dimensionless lift:

$$C_L = \gamma A S t^2 \sin(tSt), \tag{7}$$

where the dimensionless factor γ depends on C and Re and takes values around 70 within 25% for $C = 6$ and the values of Re explored.

The evolution of the wake as a function of A and St, starting before the transition to an inverted vKm wake, is shown in Fig. 6 for $Re = 100$ and $Re = 150$. Beyond the inverted vKm transition, for $StA > 0.3$ and $C = 6$, the mean drag becomes negative and the wake is deflected from the horizontal center line. As StA is increased, the distance between the tail of the foil and the point of deflection decreases, which is in agreement with other numerical simulations[2,20,26] [see Figs. 6(b), 6(c), 6(f), and 6(g)]. For $Re = 255$ and $C = 4$, the performed simulations showed the wake deflects when $StA > 0.23$, which is in good agreement with the 3D experimental observations of Godoy-Diana *et al.* in Ref. 15 and the numerical simulations in Refs. 20, 26, and 27.

The wake deflection was analyzed in detail for a fixed amplitude and a fixed Re in Ref. 20, in which the authors found that it is due to a break in the spatiotemporal symmetry; as the flapping or the amplitude is increased, asymmetric modes appear in the vorticity field. The combination between the mean flow and the symmetric and the asymmetric modes

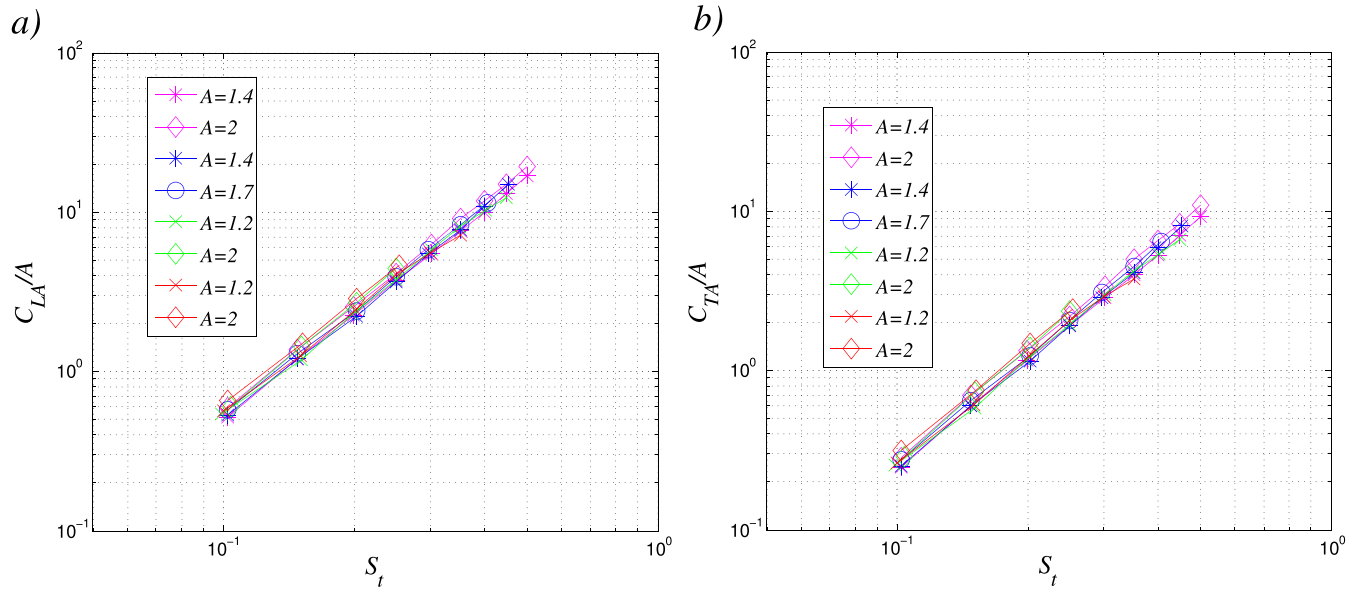

FIG. 5. Plot of (a) C_{LA} and (b) C_{TA} as functions of the St. The lines connecting points mean that A was kept constant as marked. The foil's aspect ratio is $C = 6$, and the colors represent different Reynolds numbers: magenta $Re = 50$, blue $Re = 100$, green $Re = 150$, and red $Re = 200$.

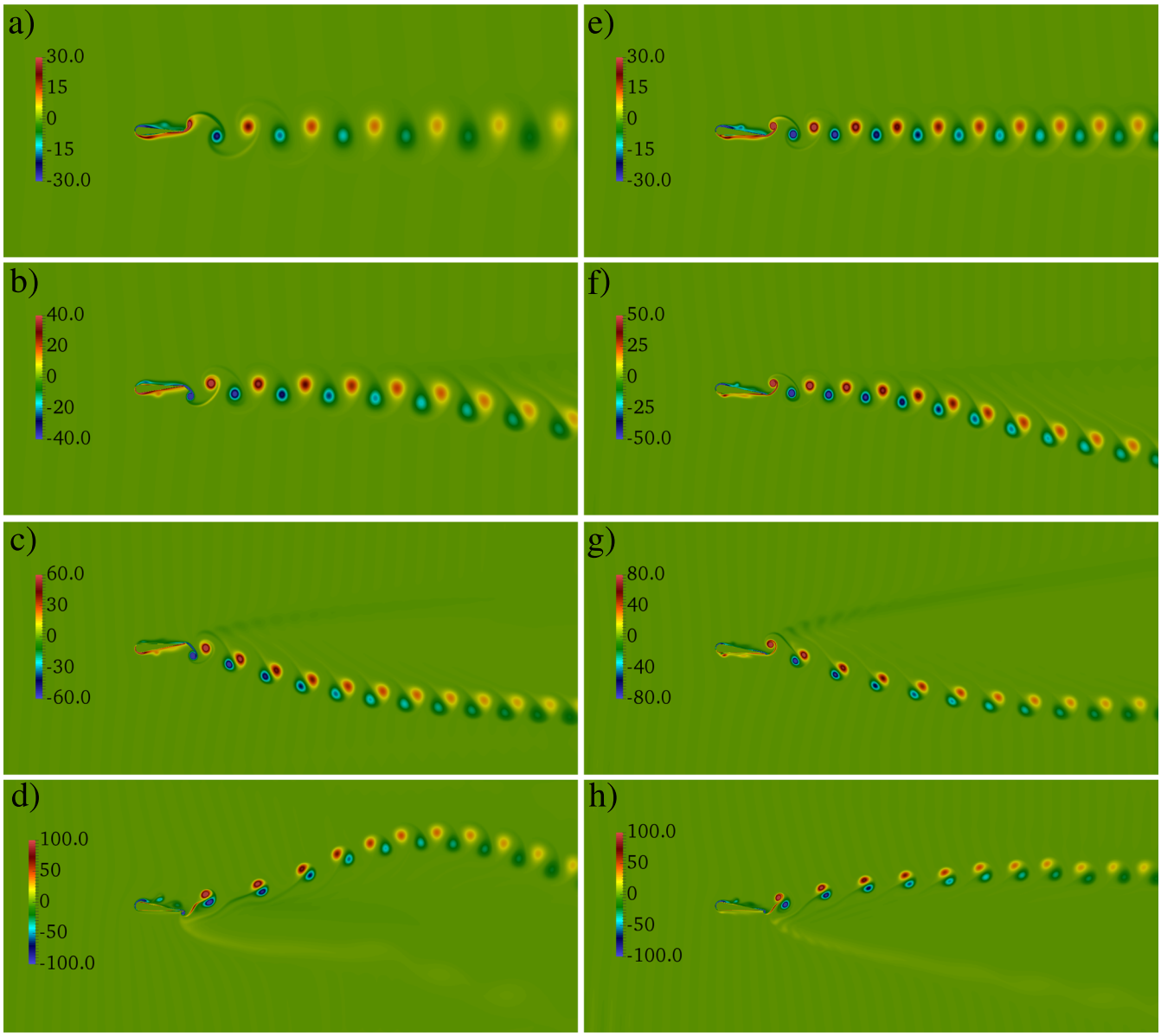

FIG. 6. Evolution of the wake for $Re = 100$ (left) and $Re = 150$ (right) with $C = 6$. (a) $StA = 2 \times 0.15 = 0.3$, (b) $StA = 1.7 \times 0.25 = 0.425$, (c) $StA = 1.2 \times 0.4 = 0.48$, (d) $StA = 1.7 \times 0.35 = 0.63$, (e) $StA = 1.2 \times 0.25 = 0.3$, (f) $StA = 1.2 \times 0.35 = 0.42$, (g) $StA = 1.4 \times 0.35 = 0.49$, and (h) $StA = 1.2 \times 0.45 = 0.54$. This figure shows the region of interest within the computational domain. Colors represent positive (red) and negative (blue) vorticity.

produce the deflection;[20] our results show that the deflection can be related to the product of ASt for a wide range of Reynolds numbers, where both inertial and viscous effects become important.

In their work, Jallas *et al.*[20] identified three regions depending on the value of the flapping frequency. The first is identified with the transition to an inverted vKm wake, the second is a transition to a deflected wake, and the third is a non-linear region characterized by the emission of dipole like vortical structures when the point of deflection reaches the trailing edge of the foil. Our numerical results are in good agreement with the tree zones for a range of moderate Reynolds numbers. We observe the transition to the inverted vKm wake, a deflection characterized by a mean lift different from zero and the shed of dipole like structures [see Figs. 6(d) and 6(h)]. However, in the third region, we observe that the wake is unstable and oscillates over long periods of time, instead of being fixed in space, as was reported in Ref. 20.

The direction of deflection is related to the initial condition;[28–30] a deflection in the opposite direction was found changing the sign of the angle $\theta_0 \to -\theta_0$. There is also a non-zero mean value of the lift coefficient that must be added in expression (7), but it is at least one order of magnitude smaller than C_L and becomes zero in the free case, as will be shown in Sec. IV B.

As StA approaches the value of 0.5, the point of deflection reaches the tail of the foil and the shed vortical structures change. This second transition was also explained in Ref. 20 in terms of non-linear effects. With each vortex pair shed, some of the vorticity is shed in the opposite angle of deflection (P + S), so one of the vortices in the pairs decreases its intensity. The hydrodynamic force remains a periodic function of time,

with the difference that C_L and C_T show only even modes, while C_D shows contribution from both even and odd modes. The angle of deflection in this regime changes with time over long flapping periods.

B. A free flapping foil

The simulations for the free foil were performed using similar initial conditions as in the fixed case. After 5×10^4 iterations, where the foil was fixed without flapping, the foil is released and starts flapping with the same exponential increase in amplitude as in the fixed case until it reaches the chosen value A. The values of $StA \in [0.1, 1.4]$ were chosen in correspondence with patterns beyond the transition to the inverted vKm wake for the fixed case.

A stationary symmetric flow without vortex shedding was observed before the foil was released. After being released, a transient time was observed where the hydrodynamic force changed from a constant value to a periodic function of time with a zero mean value. During this time interval, the center of mass accelerated until it reached an almost uniform motion in the horizontal direction with small transversal oscillations of the order of D [see Figs. 7(a) and 7(d)]. The center of mass deviates vertically a small distance from the horizontal center line during the transient, which is related to the deflection of the wake; as StA increases, this deviation decreases and the foil moves near the center line.

The motion observed after the transient does not depend on the initial condition, and the foil was also released from the final state achieved in the fixed case with the same results at long times. This protocol was chosen in order to avoid the wake left by the fixed flapping foil, which remains in the domain for several flapping periods due to its size.

The center of mass velocity is a periodic function of time. The vertical velocity oscillates with an amplitude high enough to produce an important oscillation in the vertical direction of the order of D, known as heaving [see Figs. 7(d) and 7(e)]. In other simulations found elsewhere, the profiles are forced to have a combined motion as the one observed here and then forces are measured.[5,31] We leave the discussion on differences found between the fixed and the free cases for Sec. V.

The dimensionless horizontal velocity V_x oscillates around a constant value that is a fraction of the velocity of the free stream ($U = 1$ in dimensionless units) with an amplitude that is negligible and appears to reach a practically constant value, as shown in Fig. 7(b). Since the foil reaches an almost constant value of V_x with time in all cases, V_x will be taken as its terminal average value from now on. As StA is increased, V_x diminishes until it becomes negative and the foil swims upstream. On the other hand, when StA tends to zero, the swimming velocity V_x appears to tend to one, suggesting that the foil will end up being dragged downstream with the flow.

The swimming velocity V_x is approximately a linear function of StA, as can be seen in Fig. 8(a), for most of the values of Re explored, and it failed to be so close to $Re = 50$. Therefore,

$$V_x = 1 - \gamma StA, \tag{8}$$

where the dimensionless factor γ that must depend on C has the value around 1.8 and 2.6 for the values of Re explored. This means that the foil swims upstream with a speed that grows linearly with the characteristic flapping speed $\theta_0 h\omega$ and depends slightly on the Reynolds number for $Re > 50$.

When $Re \leq 50$, the flow is dominated by viscous forces; in order to swim upstream, the product StA must be big enough to produce thrust; the slope in Fig. 8 decreases when $Re \to 0$. Therefore, this foil swims more efficiently for Reynolds numbers above the critical Re_c, where the transition from the stationary to a non-stationary flow occurs.

At the beginning of the simulations, when the foil is fixed, the horizontal force C_D reaches an almost constant value that depends on the Reynolds number [see Fig. 7(c)]. When it is

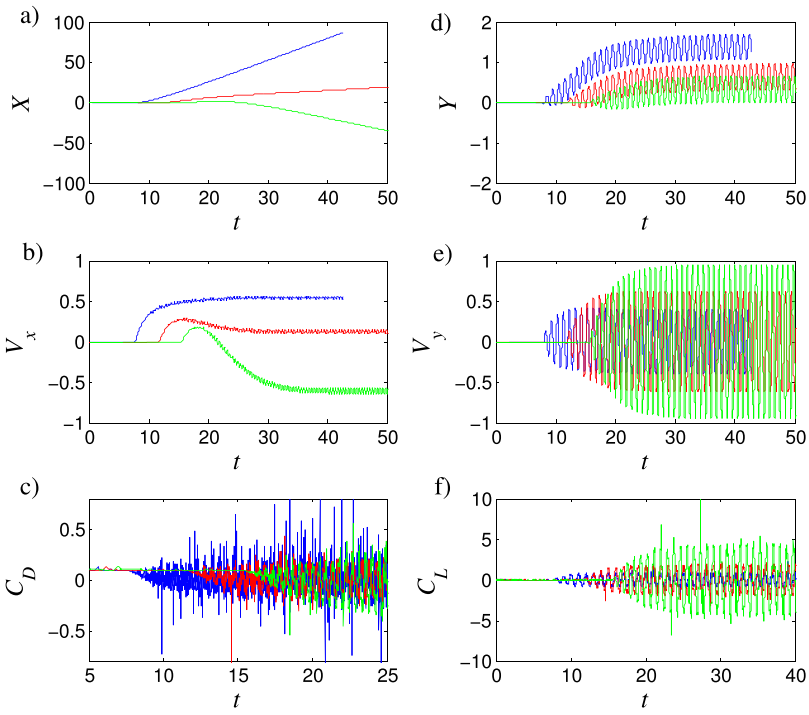

FIG. 7. Dynamics of the center of mass of the foil for $Re = 100$, $C = 6$, and $A = 1.7$: (a) the horizontal dimensionless position $X(t)$, (b) the dimensionless horizontal velocity $V_x(t)$, (c) the drag coefficient $C_D(t)$, (d) the dimensionless vertical position $Y(t)$, (e) the dimensionless vertical velocity $V_y(t)$, and (f) the lift coefficient $C_L(t)$. (Blue) $St = 0.2$, (red) $St = 0.3$, and (green) $St = 0.45$.

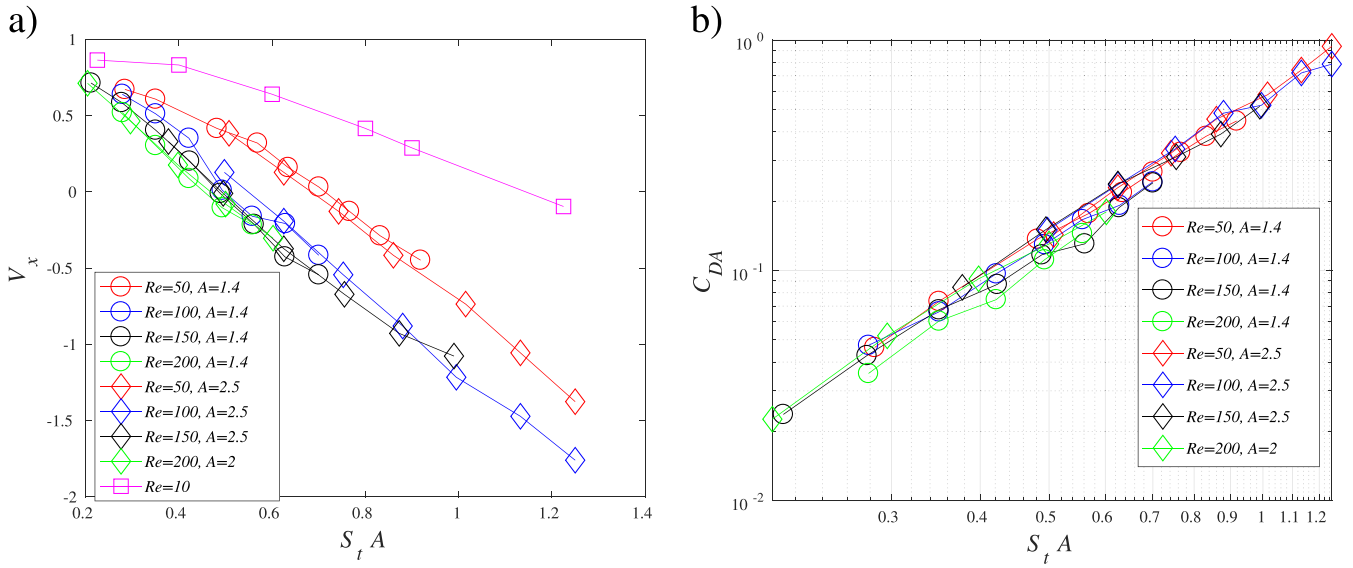

FIG. 8. Plots of the (a) swimming velocity V_x and the (b) drag amplitude C_{DA} as functions of StA for different values of the Reynolds number.

released and starts flapping, thrust is generated and C_D oscillates around a mean value tending to zero (the numerical results showed that $\langle C_D \rangle$ was of the order of 10^{-4}). The amplitude of oscillation is relatively small, and the foil reaches approximately a uniform horizontal motion, as can be seen in Figs. 7(a) and 7(b), which is consistent with the almost uniform motion observed at long times in other swimmers[12,14] in quiescent fluids.

The coefficients C_L and C_T behave similarly but with an amplitude two orders of magnitude higher [see Fig. 7(e)], which drives a notorious heaving motion shown in Figs. 7(d) and 7(e). Notice that the average value of C_L and C_T tends to zero and there is no vertical drift observed, other than that produced initially which decreases as StA is increased [see Figs. 7(d) and 7(f)]. As time passes, C_D, C_L, and C_T tend to sinusoidal, single frequency functions of time with a zero mean value.

As with the fixed foil, the long-time behavior of C_{DA} is approximately proportional to $(StA)^2$, while C_{LA} and C_{TA} grow with St^2A [see Figs. 8(b) and 9]. The freedom of translational motion produces oscillations on the hydrodynamic force of amplitude an order of magnitude smaller than those observed on the fixed foil, and so expressions (6) and (7) remain valid but for much smaller values of the factors β and γ. The first two terms in (6) must vanish to have a horizontal uniform motion, so they have to cancel each other; the drag force C_0 balances the trust produced by the flapping. On the contrary, C_{TA} is of the same order in both cases as the swimming foil is not free of rotational motion.

This suggests that imposing the motion of a foil introduces significant differences in the observed flow and forces when compared to a self-propelled swimmer. Additionally, the fact that in the free case, hydrodynamic forces are smaller than their counterparts in the fixed case (see Fig. 11) allowed us to

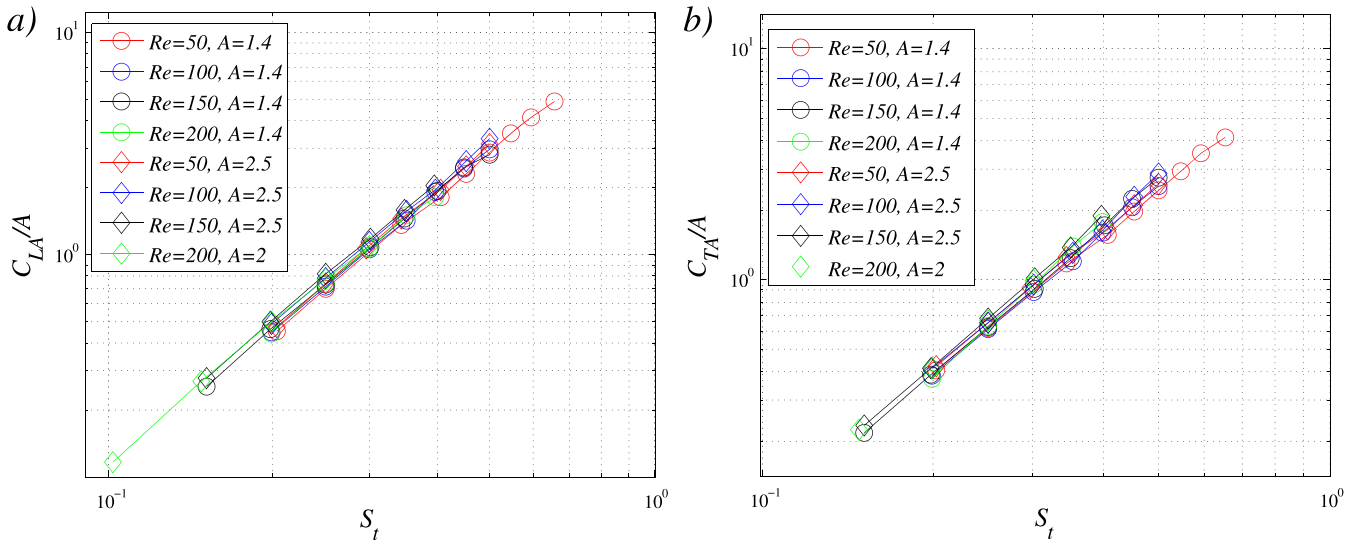

FIG. 9. Plots of (a) C_{LA}/A and (b) C_{TA}/A as functions of St for different values of the Reynolds number.

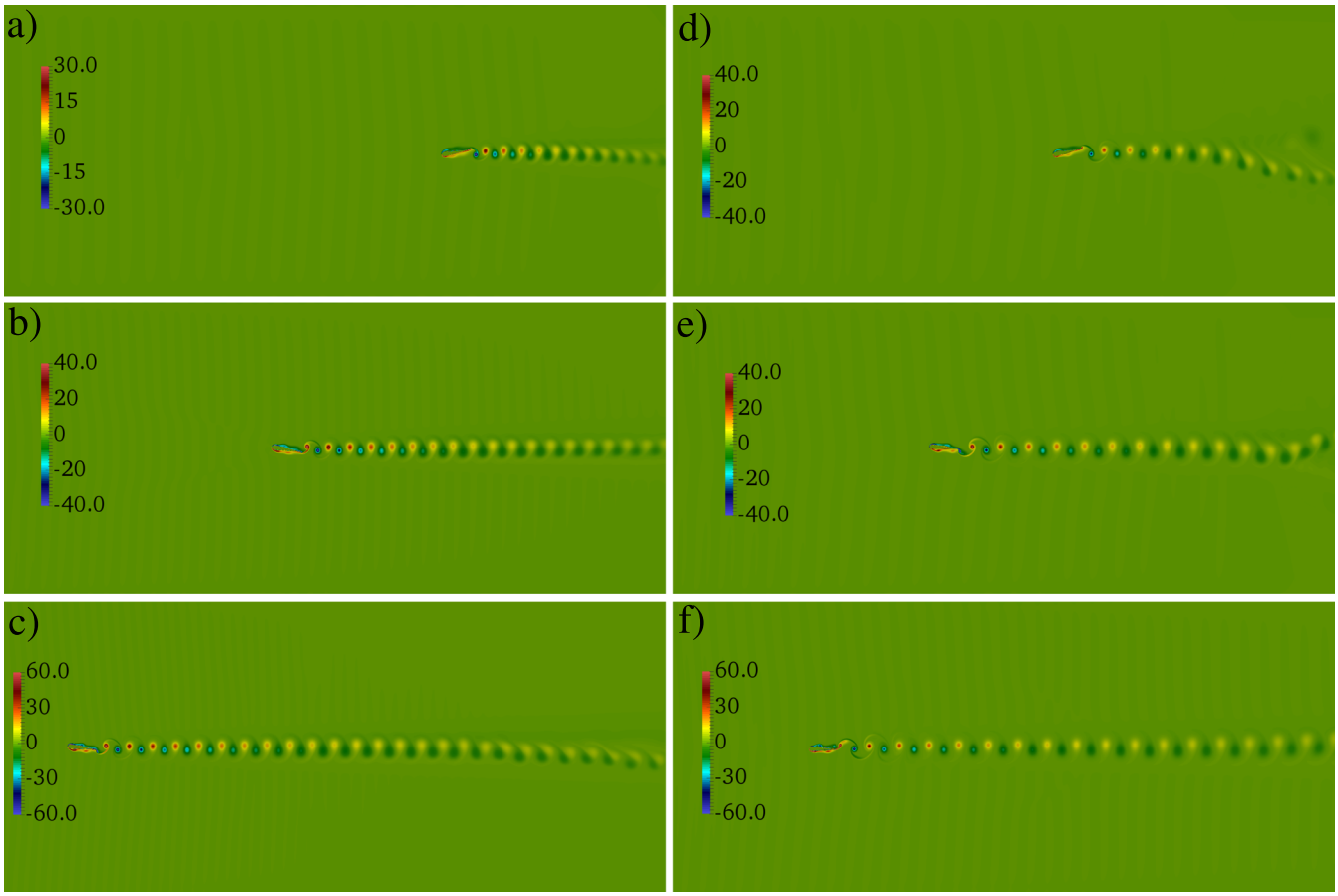

FIG. 10. Vorticity distribution for a moving flapping foil for $C = 6$, $Re = 100$, and $A = 2$ (left) and $Re = 150$ and $A = 2.5$ (right). Colors represent positive (red) and negative (blue) vorticity. (a) $St = 0.2$ and $V_x > 0$, (b) $St = 0.3$ and $V_x \sim 0$, and (c) $St = 0.4$; the foil swims upstream with $V_x < -1$. (d) $St = 0.25$ and $V_x > 0$, (e) $St = 0.35$ and $V_x \sim 0$, and (f) $St = 0.45$; the foil swims upstream with $V_x < -1$. These figures show the complete computational domain, and the initial position is different in each case.

explore larger values of Re, St, and A in the free case than in the fixed one.

As expected, the free foil retains the inverted vKm wake, as shown in Fig. 10. The deflection of the wake observed in the fixed foil now appears with the first strokes and is dragged away from the swimmer. When V_x is positive, the flapper is unable to swim upstream [Fig. 10(a)], the point of deflection moves away a few lengths C from the tail's tip before the foil and the wake are dragged out of the domain on the left side. As StA increases and V_x reaches zero, the point of deflections moves further away from the tail, contrary to what happens to the fixed flapping foil (see Sec. IV A).

As was already mentioned above, the deflection was accompanied by a non-zero mean lift coefficient and its direction with the initial condition in the fixed case. When the foil is free of translational motion, it has a small lateral drift in the acceleration period and then oscillates (the heaving) around a constant value. The mean value of all the force coefficients becomes zero, so the deflection is only an artefact of the initial condition and gets swept away eventually.

The cases $V_x = 0$, corresponding to the values of StA between 0.4 and 0.7, depending on Re [see Fig. 8(a)], differ from the flow around the fixed flapping foil with the same StA and Re values in their heaving motion, and in that, the wake deflection disappears. As we continue increasing StA, $V_x < 0$ and the foil swims upstream with a horizontal speed proportional to StA and with an increased amplitude of heaving.

V. DISCUSSION

As already noticed, the fixed and free flappers share some common features. When the free flapper reaches its terminal horizontal speed, in both cases, the proportionality of C_D and C_L on $(StA)^2$ and St^2A, respectively, is observed. This suggests the use of the drag on the fixed flapper (6) to propose a relation of the thrust behavior and its relation to V_x. If we take the mean value of C_D from Eq. (6) and assume that the horizontal hydrodynamic force tends to zero when freed [see Fig. 7(c)] because the horizontal speed becomes practically constant, then the dimensionless thrust, say C_t, corresponds to the negative term proportional to $(StA)^2$ and must balance the drag C_0. Then using relation (8), we propose the proportionality

$$C_0 \propto (1 - V_x)^2, \tag{9}$$

which satisfies that drag is zero when there is not flapping at all and the fluid drags the foil downstream.

In the fixed case, the mean value of C_D is, in general, different from zero; it measures the mean force produced at the center of mass in order to keep it at rest. Depending on

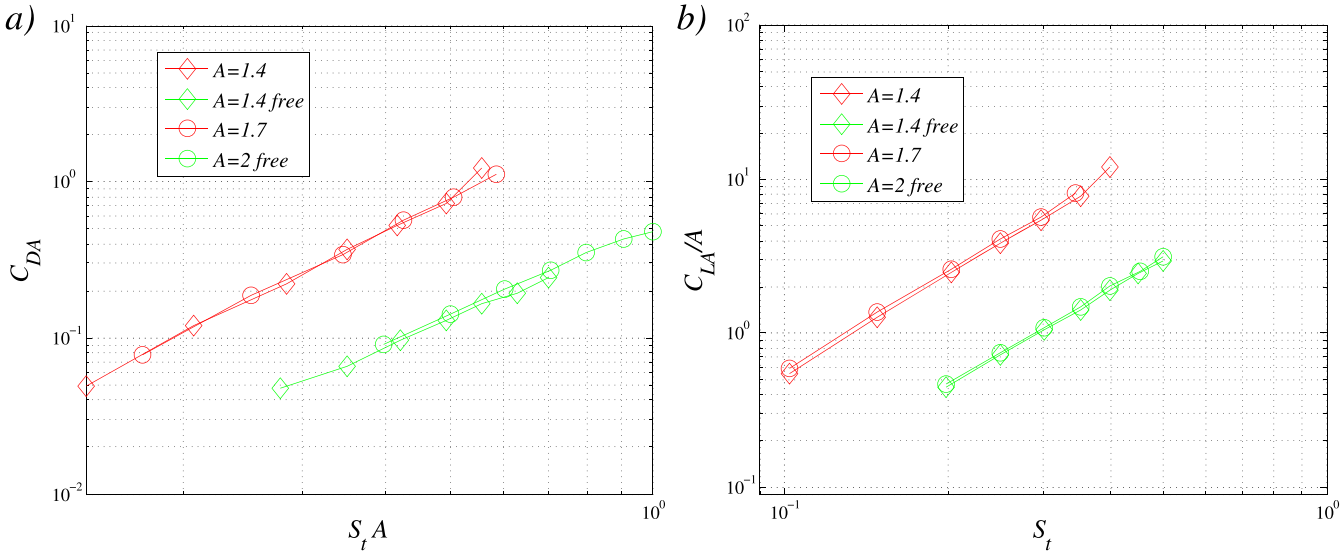

FIG. 11. Drag and lift coefficients as a function of *St* and *A* for the free case (green) and for the fixed case (red). The joined points represent experiments made at fixed values of *A* and varying *St*.

the value of *Re* and *StA*, this force can be negative or positive depending on the difference between the drag C_0 and C_t; the mean force is zero at a particular value of *StA* in contrast to the free case where it is always zero. If the foil is released, it moves with a combination of uniform horizontal motion and vertical heaving, due to the response of the fluid to its imposed rotation, which diminishes the magnitude of the local stresses on the foil's surface, as is shown in Fig. 11, by an order of magnitude. The constraint force underneath the condition for the foil's center of mass to be fixed in space corresponds to the reaction on the flow stresses found numerically, showing larger amplitudes of oscillations when compared to the free foil.

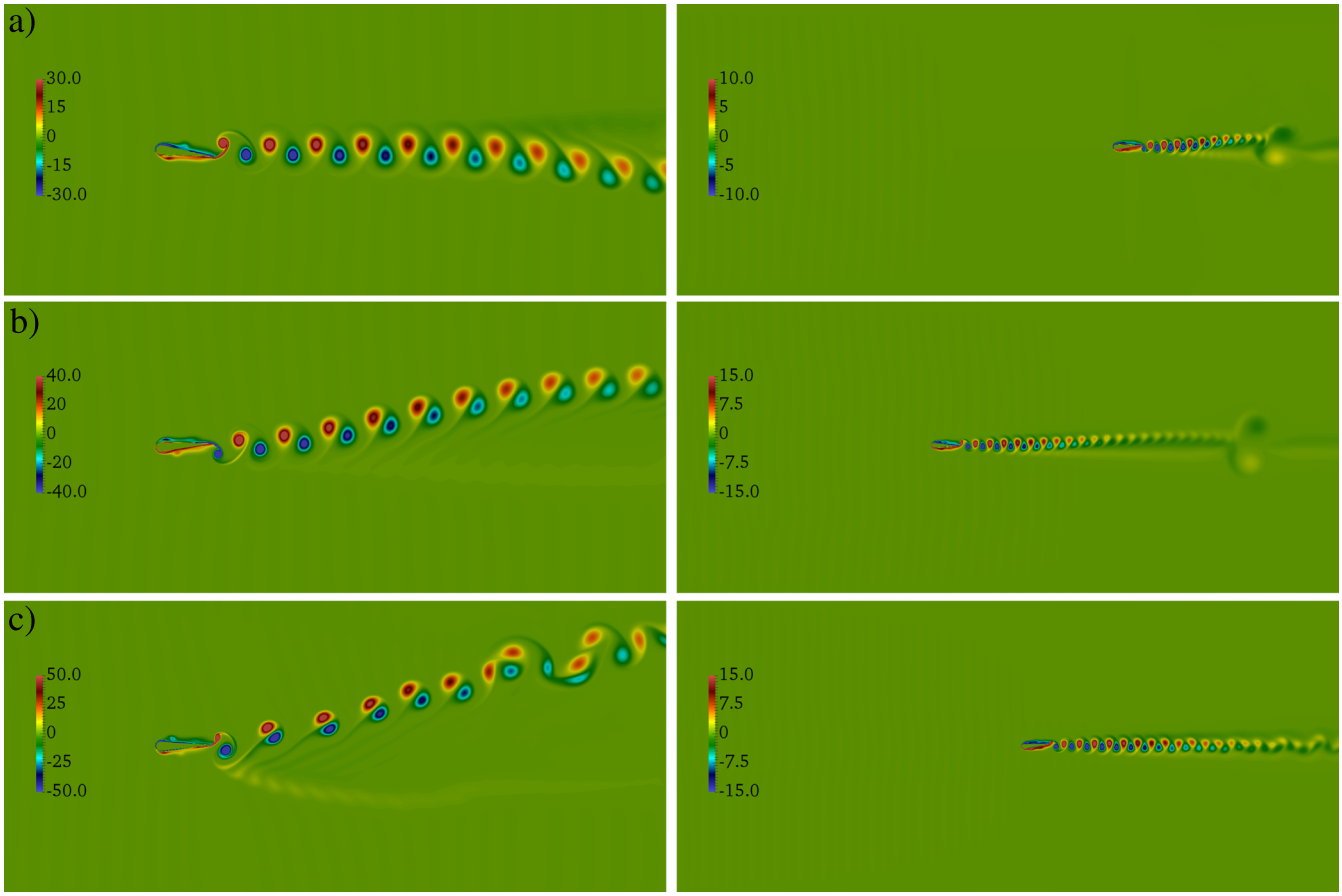

FIG. 12. Comparison between the wake observed in the fixed (left) and the free (right) cases for $Re = 100$. The amplitude was kept fixed at $A = 1.4$. (a) $St = 0.3$ and $V_x > 0$, (b) $St = 0.35$ and $V_x \sim 0$, and (c) $St = 0.4$ and $V_x < 0$.

The constraint force prevents the heaving motion observed when the foil is released and balances the mean lift observed in the fixed flapper.[20] As *StA* increases, the constraint force on the fixed flapper must grow along with flow stresses, producing the observed instabilities on the flow structure.

The wake structure on the free foils, the swimmers, is stable for all the parameter values explored (see Fig. 12). In the cases where the swimmer is dragged by the uniform flow, the wake is shorter and shows a deflection produced with the initial flapping that gets swept away. The parameter values for the free foil swimming upstream correspond to those of the unstable wake for the fixed case [see Figs. 12(b) and 12(c)]. In these cases, the foil has enough time to develop its wake before leaving the computational domain. A small deflection of the wake, produced at the beginning of the flapping motion, is dragged away from the swimmer, and its wake ends up being practically symmetrical.

VI. CONCLUSIONS

In this work, numerical results on the two-dimensional incompressible viscous flow around a rigid flapping foil are presented. Both a fixed flapping foil and a flapping foil free of translational motion were considered. The flow field was computed using a lattice Boltzmann model that includes a procedure for moving internal boundaries with an arbitrary geometry, thus allowing the computation of the translational motion of a free foil due to hydrodynamic forces. The numerical results were compared with experimental[1,15] and other computational results.[2,20,26]

The swimming speed increased linearly with the flapping speed $\theta_0 h\omega$, and for Reynolds numbers around and above 100, this speed seemed to depend only on *StA*. On the contrary, for *Re* of the order of 10, a stronger flapping was needed to obtain swimming speeds slightly less than one, showing the importance of viscous effects. As swimming at an almost constant horizontal speed comes with an approximate balance between drag and thrust, together with the linear dependence of V_x on *StA* found, we were able to propose that drag (and trust) is proportional to the square of the relative speed $(V_x - 1)$ in the free case.

The wake behind both the fixed and the free flappers showed a deflection. Contrary to the fixed flapper, the free foil swimming upstream produces a wake with a smaller deflection within the first strokes. This initial condition effect, the wake deflection, is eventually left behind and swept away from the foil, and so the swimmer ends up having a symmetrical wake. The hydrodynamic force in this case has zero mean value, which relates to a vorticity field that will become symmetric eventually, in contrast to the fixed case, where the mean hydrodynamic force is different from zero and the vorticity field has asymmetric modes.

ACKNOWLEDGMENTS

Partial support from Project Nos. UNAM-PAPIIT-IN115216 and IN115316 is acknowledged. The authors thank Dr. Eduardo Ramos and Dr. Raúl Rechtman for their support.

[1] T. Schnipper, A. Andersen, and T. Bohr, "Vortex wakes of a flapping foil," J. Fluid Mech. **633**, 411 (2009).
[2] A. Das, R. K. Shukla, and R. N. Govardhan, "Existence of a sharp transition in the peak propulsive efficiency of a low pitching foil," J. Fluid Mech. **800**, 307 (2016).
[3] J. Wu, Y. L. Chen, and N. Zhao, "Role of induced vortex interaction in a semi-active flapping foil based energy harvester," Phys. Fluids **27**, 093601 (2015).
[4] T. Y. Wu, "Extraction of flow energy by a wing oscillating in waves," J. Ship Res. **16**, 66 (1972).
[5] J. M. Anderson, K. Streitlien, D. S. Barrett, and M. S. Triantafyllou, "Oscillating foils of high propulsive efficiency," J. Fluid Mech. **360**, 41 (1998).
[6] H. Dong, R. Mitall, and F. M. Najjar, "Wake topolgy and hydrodynamic performance of low-aspect-ratio flapping foils," J. Fluid Mech. **566**, 309 (2006).
[7] M. S. Triantafyllou, G. S. Triantafyllou, and D. K. P. Yue, "Hydrodynamics of fishlike swimming," Annu. Rev. Fluid Mech. **32**, 33 (2000).
[8] G. K. Taylor, R. L. Nudds, and A. L. R. Thomas, "Flying and swimming animal cruise at a Strouhal number tuned for high power efficiency," Nature **425**, 707 (2003).
[9] N. Vanderberghe, J. Zhang, and S. Childress, "Symmetry breaking leads to forward flapping flight," J. Fluid Mech. **506**, 147 (2004).
[10] S. Alben and M. Shelley, "Coherent locomotion as an attracting state for a free flapping body," Proc. Natl. Acad. Sci. U. S. A. **102**, 11163 (2005).
[11] N. Vanderberghe, S. Childress, and J. Zhang, "On unidirectional flight of a free flapping wing," Phys. Fluids **18**, 014102 (2006).
[12] S. Kern and P. Koumoutsakos, "Simulations of optimized anguilliform swimming," J. Exp. Biol. **209**, 4841 (2006).
[13] B. J. Gemmell, S. P. Colin, J. H. Costello, and J. O. Dabiri, "Suction-based propulsion as a basis for efficient animal swimming," Nat. Commun. **6**, 8790 (2015).
[14] N. G. Chisholm, D. Legendre, E. Lauga, and A. S. Khair, "A squirmer across Reynolds numbers," J. Fluid Mech. **796**, 233 (2016).
[15] R. Godoy-Diana, J.-L. Aider, and J. E. Wesfreid, "Transitions in the wake of a flapping foil," Phys. Rev. E **77**, 016308 (2008).
[16] X. He, S. Chen, and G. D. Doolen, "A novel thermal model for the lattice Boltzmann method in incompressible limit," J. Comput. Phys. **146**, 282 (1998).
[17] F. Mandujano and R. Rechtman, "Thermal levitation," J. Fluid Mech. **606**, 105 (2008).
[18] J. R. Clausen, D. A. Reasor, and C. K. Aidun, "Parallel performance of a lattice-Boltzmann/finite element cellular blood flow solver on the IBM Blue Gene/P architecture," Comput. Phys. Commun. **181**, 1013 (2010).
[19] P. Vorovieff, D. Georgiev, and M. S. Ingber, "Onset of the second wake: Dependence on the Reynolds number," Phys. Fluids **14**, L53 (2002).
[20] D. Jallas, O. Marquet, and D. Fabre, "Linear and nonlinear perturbation analysis of the symmetry breaking in time-periodic propulsive wakes," Phys. Rev. E **95**, 063111 (2017).
[21] A. W. Mackowski and C. H. K. Williamson, "Effect of pivot location and passive heave on propulsion from a pitching airfoil," Phys. Rev. Fluids **2**, 013101 (2017).
[22] Z. Guo and C. Zheng, "An extrapolation method for the boundary conditions in the lattice Boltzmann method," Phys. Fluids **14**, 2007 (2002).
[23] R. Mei, D. Yu, W. Shyy, and L. Luo, "Force evaluation in the lattice Boltzmann method involving curved geometry," Phys. Rev. E **65**, 041203 (2002).
[24] C. H. K. Williamson and R. Govardhan, "Vortex induced vibrations," Annu. Rev. Fluid Mech. **36**, 413 (2004).
[25] T. von Kármán and J. M. Burgers, *General Aerodynamic Theory: Perfect Fluids* (Dover Publications, 1963; 1935).
[26] J. Deng and C. P. Caulfield, "Three-dimensional transition after deflection behind a flapping foil," Phys. Rev. E **91**, 043017 (2015).
[27] G.-Y. He, Q. Wang, X. Zhang, and S.-G. Zhang, "Numerical analysis on transitions and symmetry breaking in the wake of a flapping foil," Acta Mech. Sin. **28**, 1551 (2012).
[28] J. C. S. Lai and M. F. Platzer, "Jet characteristics of a plunging airfoil," AIAA J. **37**, 1529 (1999).
[29] K. D. von Ellenrieder and S. Pothos, "PIV measurements of the asymmetric wake of a two-dimensional heaving hydrofoil," Exp. Fluids **44**, 733 (2008).
[30] Z. C. Zheng and Z. Wei, "Study of mechanisms and factors that influence the formation of vortical wake of a heaving airfoil," Phys. Fluids **24**, 103601 (2012).
[31] A. Mivehchi, J. Dahl, and S. Licht, "Heaving and pitching oscillating foil propulsion in ground effect," J. Fluids Struct. **63**, 174 (2016).